Clays and Clay Minerals, Vol. 62, No. 4, 253–266, 2014.

ASSESSMENT OF PEDOGENIC GIBBSITE AS A PALEO-PCO_2 PROXY USING A MODERN ULTISOL

JASON C. AUSTIN* AND PAUL A. SCHROEDER

University of Georgia, Department of Geology, Athens, GA 30602-2501 USA

Abstract—The stable carbon isotope composition of CO_2 occluded in the gibbsite structure is proposed as a potential atmospheric paleo-PCO_2 proxy. Analysis of pedogenic gibbsite from a modern Ultisol in the Piedmont of Georgia, USA, was conducted to test the basis for this concept and to help constrain the parameters used to describe physical and biological processes affecting such factors as the respiration rate of CO_2. Co-variation of the $\delta^{13}C$ and $\delta^{18}O$ values with depth along a gradient parallel to the mixing line between the atmosphere and the soil organic material implies that diffusion is the process that determines the stable isotope composition of soil CO_2. In the upper 40 cm, the measured $\delta^{13}C$ values are not consistent with the expected diffusive depth profile assumed in paleo-PCO_2 models. The isotope signature is reset downward in the depth profile with a concentration of the most atmosphere-like $\delta^{13}C$ and $\delta^{18}O$ values occurring at the top of the Bt horizon by some as-yet-unknown process. Bioturbation, recrystallization, and physical translocation are potential explanations for this observation. Regardless of the process at work, the net effect is an apparent two-component mixing curve between the top of the Bt horizon and deep within the saprolite. In cases where the A horizon is eroded but the Bt horizon is preserved it is possible that $\delta^{13}C$ values of gibbsite-occluded CO_2 can serve as a proxy for atmospheric paleo-PCO_2. Careful textural study of all paleosols is therefore essential to match stable carbon isotope signatures with the horizons preserved. Understanding of modern dynamics and preservation of these isotopic signatures may also be important for those that employ other carbonate proxies.

Key Words—Paleo-PCO_2 Proxies, Pedogenic Gibbsite, Soil CO_2 Diffusion, Stable Carbon Isotopes, Stable Oxygen Isotopes, Ultisol.

INTRODUCTION

A review of proxy-based estimates of paleo-PCO_2 through geologic time reveals a large range of error associated within individual methods and a large range of estimates between methods (Royer *et al*., 2001). Paleo-PCO_2 proxies using marine phytoplankton and a stomatal index have small estimated errors (200 and 50 ppmv, respectively) but are temporally limited to Cretaceous and younger samples. In addition, these proxies are reliable only under relatively low atmospheric PCO_2 conditions (1250 and 340 ppmv, respectively) (Farrimond *et al*., 1986; Woodward and Bazzaz, 1988; Marlowe *et al*., 1990; Freeman and Hayes, 1992; Van Der Burgh *et al*., 1993; Kurschner *et al*., 1996; Kump and Arthur, 1999; Pagani *et al*., 1999; Royer *et al*., 2001). Pedogenic carbonates provide information over the much longer history of soils on earth (*i.e.* the Phanerozoic) formed in arid environments. However, uncertainty in estimating the concentration of CO_2 in the soil results in large errors. When compared to other methods such as the GEOCARB model (Berner and Kothavala, 2001) the pedogenic carbonate method appears to over-estimate paleo-PCO_2 (Breecker *et al*., 2009); the latter authors suggested that better agreement is possible if seasonal biases for time of mineralization are factored into model assumptions. Pedogenic goethite has also been used as a proxy but is limited to Fe-rich, wet climates mutually exclusive of arid calcrete-forming environments (Yapp and Poths, 1992, 1996). Direct comparison of proxy-derived paleo-PCO_2 estimates are limited by the effective time and spatial ranges of each proxy. Other, independent proxies effective over broad age ranges would therefore be helpful. Recent work modeling the stable carbon isotope composition of a carbonate-like component associated with pedogenic gibbsite suggests that this mineral has the potential to fill the proxy need (Schroeder *et al*., 2006; Austin, 2011).

The pedogenic gibbsite proxy employs the same Fickian diffusion model developed for pedogenic carbonates by Cerling (1984) and is described in detail by Austin (2011) who used both analytical and numerical approaches to evaluate errors. Briefly, the diffusion model takes the form:

$$\frac{\partial C_s^*}{\partial t} = D_s^* \frac{\partial^2 C_s^*}{\partial z^2} + \phi_s^*(z) \qquad (1)$$

where C is the concentration of CO_2 in the soil, D is the diffusion coefficient, t is time, z is depth, and ϕ is the production rate of CO_2 in the soil as a function of depth. Subscript 's' refers to the soil and * refers to bulk CO_2 as

* E-mail address of corresponding author:
jaycaustin@live.com
DOI: 10.1346/CCMN.2014.0620402

opposed to ^{12}C or ^{13}C. The general solution of this equation is

$$C_s^*(z) = S(z) + C_a^* \quad (2)$$

where $S(z)$ is the concentration of CO_2 in the soil and C_a^* is the bulk concentration of CO_2 in the atmosphere. The production rate function can take different forms depending on the assumptions made about how CO_2 production varies with depth (ϕ_s^* in equation 1) (Cerling, 1999). The pedogenic gibbsite proxy is most sensitive to the soil respiration rate, which is dependent on the diffusion coefficient and soil CO_2 production rate, and the $\delta^{13}C$ value of the soil organic material (SOM) that is producing CO_2 in the soil. To assess the applicability of the model to CO_2 occluded in the gibbsite structure, a field test was conducted on an active Ultisol for comparison to a similar data set (Schroeder and Melear, 1999). The field test also enabled a more detailed evaluation of the general applicability of modeling assumptions related to the physical properties of the soil including porosity, tortuosity, and the $\delta^{13}C$ value of the soil biomass. The utility of the model will be increased if the general assumptions for parameters such as soil bulk density, tortuosity, and CO_2 production rate worked equally well for two sites with similar soil types and vegetation.

CO_2 collected during the dehydration of gibbsite is assumed to be liberated from defect sites where it is trapped during mineral formation in the soil. Bidentate carbonate anions have been shown to adsorb strongly to the surface of goethite and gibbsite (Su and Suarez, 1997). The nature of CO_2 incorporation differs from the cases of soil carbonate and goethite where the CO_2 is assumed to be part of the mineral structure. Infrared (IR) spectroscopy suggests that carbonate is present in goethite as a solid solution and is accommodated in an open channel parallel to the c^* axis (Yapp and Poths, 1990). The crystalline structure of gibbsite does not have the required space to accommodate a carbonate ion. In addition, the charge imbalance resulting from the exchange of an OH^- with a CO_3^{2-} ion prohibits a solid solution. A constant ratio yield (*i.e.* CO_2 to H_2O) during mineral dehydration/decarbonation at ~230ºC under vacuum demonstrates the stoichiometric breakdown of the goethite structure (Yapp and Poths, 1986). $Fe(O_{1-X},(CO_3)_X)OH$ (where X = moles of occluded CO_2) as shown by the reaction

$$Fe(O_{1-X})(CO_3)_XOH \rightarrow \tfrac{1}{2}\, Fe_2O_3 + \tfrac{1}{2}\, H_2O + XCO_2 \quad (3)$$

Alternatively as,

$$(1-X)FeOOH + XFeCO_3OH \rightarrow \tfrac{1}{2}\, Fe_2O_3 + \tfrac{1}{2}\, H_2O + XCO_2 \quad (4)$$

Similar stoichiometric responses for CO_2 yields from gibbsite have also been documented (Schroeder and Melear, 1999). The reaction below shows the stoichiometric C/H yielded at ~230ºC under vacuum.

$$Al(OH)_3XCO_2 \rightarrow \tfrac{1}{2}\, Al_2O_3 + \tfrac{3}{2}\, H_2O + XCO_2 \quad (5)$$

Values for X in goethite are related to F, which is defined as the molar ratio of CO_2:H_2O. Constant values of F during step-wise extraction of natural goethite range up to 0.01 (Yapp and Poths, 1991; Yapp, 1997) and values for natural gibbsite range up to 0.005 (Tabor and Yapp, 2005). Note that if similar numbers of moles of carbon are occluded in both minerals, then the C/H is smaller for gibbsite because of the greater water yield. Due to the presence of three possible OH^- sites for CO_3^{2-} anion bonding in gibbsite as compared to the single O^{2-} site in goethite, it is expected that on a molar basis gibbsite will have a greater capacity for carbon sequestration. In fact, comparison of CO_2 yield (μmoles CO_2/mg sample) for published values of both goethite and gibbsite shows that the ratio of gibbsite CO_2: goethite CO_2 is ~3:1 (Tabor and Yapp, 2005; Yapp and Poths, 1991).

The $\delta^{13}C$ values observed by Schroeder and Melear (1999) suggest diffusion-controlled soil atmosphere mixing. Analytical and numerical modeling predicted a soil respiration rate which is an order of magnitude slower than the measured rate (Schroeder *et al*., 2006). The present study proposes that the concomitant $\delta^{18}O$ composition of the CO_2 may give additional insight into the process controlling the isotopic signatures of CO_2 occluded in gibbsite and the possibility to detect exchange of isotopes with the environment after mineral formation, a process that could compromise the $\delta^{13}C$ proxy.

The $\delta^{18}O$ compositions of soil CO_2 have been studied extensively because they are useful for modeling the carbon cycle, where it has been shown that the soil is a large reservoir that contributes CO_2 to the atmosphere (Hesterberg and Siegenthaler, 1991; Miller *et al*., 1999; Stern *et al*., 1999). The oxygen isotopic composition of CO_2 produced in soil by plant and microbial respiration is expected to be in equilibrium with soil water because the soil water is assumed to be the same inside and outside the roots (Cuntz *et al*., 2003). The $\delta^{18}O$ value of soil CO_2 is controlled by diffusion through the soil and the isotope exchange reaction between soil water and soil gas CO_2. $^{12}C^{16}O^{18}O$ has a slower diffusivity than $^{12}C^{16}O_2$ due to its greater mass. Differences in mass-dependent diffusion rates result in an enrichment of 8.7‰ in soil CO_2 if diffusion is the only process controlling the $\delta^{18}O$ value (Miller *et al*., 1999). The relatively rapid exchange of oxygen atoms occurs in the reaction,

$$^{12}C^{16}O^{16}O + H_2^{18}O \rightarrow {}^{12}C^{16}O^{18}O + H_2{}^{16}O \quad (6)$$

Quasi-equilibrium exists between the soil water and the enriched soil CO_2. Experimental work under rate-limiting conditions showed that this reaction will reach equilibrium in 110 s at 25ºC (Stern *et al*., 1999). In soils however, this reaction usually does not reach

https://doi.org/10.1346/CCMN.2014.0620402 Published online by Cambridge University Press

equilibrium due to the transport-limiting nature of the soil pore networks (Hsieh *et al*., 1998). Therefore, the expected $\delta^{18}O$ of the soil CO_2 is expected to be enriched by some amount less than 8.7‰ compared to soil water, depending on the rate of the isotope exchange reaction.

Note that in experiments conducted on goethite, the $\delta^{18}O$ values of CO_2 extracted during dehydration varied as a function of the reaction rate (Yapp, 2003). The variation is the result of exchange between the liberated CO_2 and H_2O. A similar result has been shown for kaolinite and dickite (Girard and Savin, 1996). Fractionation of oxygen isotopes during dehydration calls into question the validity of conclusions regarding the co-variation of $\delta^{18}O$ and $\delta^{13}C$ values in this study. The $\delta^{18}O$ data are presented here and the implications of these questions are discussed in detail.

The purpose of the present study was to examine the $\delta^{13}C$ and $\delta^{18}O$ compositions of CO_2 occluded in gibbsite in an active soil profile with the aim of assessing the validity of using this signature as a paleoclimate proxy in paleosols.

SITE DESCRIPTION AND METHODS

The sampling location is a moderately dense deciduous forest located in the J. Phil Campbell Natural Resource Conservation Center, Watkinsville, Georgia, USA, which has been operated by the USDA-ARS since 1937 (33º51′55″N, 83º27′23″W). Historical aerial photography and anecdotal evidence from local farmers confirm that the ~3.5 acre (1.4 hectare) plot has been fenced and managed as a forest for more than a century and escaped cotton management and tillage. Plants using a C_3 photosynthetic carbon fixation pathway are assumed to be the only input of respired CO_2. This site was selected specifically to mitigate contributions from carbon isotope pools that may have been generated using other pathways (*i.e.* C_4). The parent-rock material is the Athens Gneiss and the soil is identified as CYB2 (Cecil series soil eroded, with up to 2% slope) (Robertson, 1968). This field location was also chosen for its relatively high landscape position, to minimize colluvial inputs from other locations in the watersheds sited at the experiment station.

Soil material was excavated from a 1 m^2 square area at discrete depth layers (*e.g.* 0–5 cm, 5–10 cm, *etc.*). Each layer was removed using a hand trowel and packed into 5-gallon buckets, which were then closed and sealed and stored in the field before processing at the laboratory. The sample at the top of the O_a horizon (0–5 cm depth) was taken after removal of large, loose, leaf litter which consisted mostly of organic material with some mineral material. Minor sampling overlap occurred between the 5–10 cm and 10–20 cm segments due to heterogeneities in the pit. Beyond 20 cm, to a depth of 100 cm, the pit was dug over a period of three months with more accurate depth control. Additional samples beyond 100 cm depth were collected from three peripheral auger cores extracted ~1 m from the pit edges. Auger core samples were used along with the pit sample splits to determine percent sand, silt, and clay (by weight) using standard sieve and settling-tube methods. Bulk-sample stable carbon isotope composition and percent organic carbon analysis was performed prior to chemical treatment at the University of Georgia Stable Isotope & Soil Biology Lab (http://swpa.uga.edu) using standard tin capsules, micro-Dumas combustion, a Thermo Finnigan Delta V, Isotope Ratio Mass Spectrometer (Bremen, Germany) coupled to a Carlo Erba NA1500 CHN Analyzer (Milan, Italy) *via* a Thermo Finnigan Conflo III Interface, and standards (relative to Vienna Pee Dee Belemnite).

The <2 μm size fraction was treated chemically with 0.5 M HCl and 30% H_2O_2 following the methods described by Yapp and Poths (1996) and Schroeder and Melear (1999) to produce ~300–500 g of sample mass. X-ray diffraction (XRD) analyses were performed using a Bruker D8 Advanced diffractometer (Co radiation). All samples were examined before and after chemical treatments to verify that no change in mineralogy had occurred as a result of the chemical treatment. No peaks for carbonates in the original diffraction patterns of any sample material were observed. Ratios of gibbsite (002) peak height to the kaolinite (001) peak height were calculated and defined as the mineral index (Figure 1) to allow comparison of the relative abundance of gibbsite at different depths in the soil.

The treated sample material was heated in a step-wise procedure to allow for the collection of CO_2 liberated from the mineral structure during the thermal breakdown of gibbsite and goethite following the procedure of Schroeder and Melear (1999) in the University of Georgia Stable Isotope Laboratory. During sample collection, the CO_2 was separated cryogenically from the co-evolved H_2O using a dry ice ethanol mixture.

The CO_2 collected was analyzed by conventional dual inlet mass spectrometry using a Finnigan MAT 252 (Thermo, USA) instrument equipped with a microvolume coldfinger for the stable carbon and oxygen isotope ratios. The volume of CO_2 analyzed ranged from 20 to <1 micromoles (μmol). The stable carbon isotope ratios were plotted to determine the plateau $\delta^{13}C$ value, which indicates stoichiometric breakdown and that the CO_2 originates from a single pool assumed to be trapped CO_2 in the gibbsite structure.

RESULTS

Textural analysis returned values typical of the regional Cecil-series soil, with the maximum % clay (63%) occurring at the top of the Bt horizon (30–50 cm) (Figure 1, Table 1). The wt.% organic carbon reached a maximum of 6% at the surface and the $\delta^{13}C$ value of the

https://doi.org/10.1346/CCMN.2014.0620402 Published online by Cambridge University Press

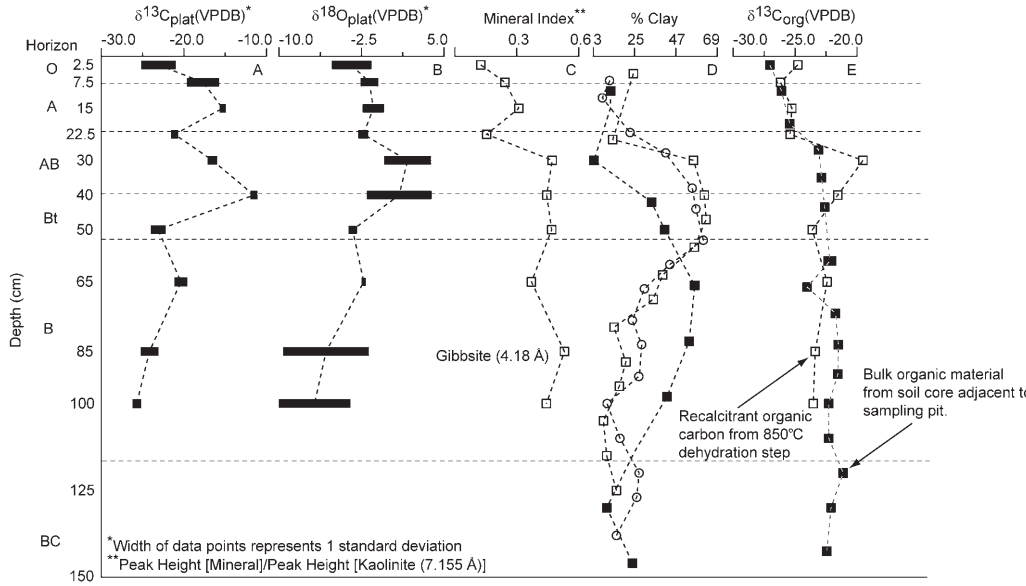

Figure 1. Compilation of all data collected from the field site: (A) $\delta^{13}C$ values of plateaus from the dehydration process (the width of the box represents variability in the results from multiple analyses); (B) $\delta^{18}O$ values of plateaus from the dehydration process (the width of the box represents variability in the results from multiple analyses); (C) mineral index defined as the XRD peak height of gibbsite as a ratio with kaolinite peak height; (D) percentage of clay determined from three soil cores located 1 m from the soil pit; (E) $\delta^{13}C$ values of bulk SOM (filled squares) and the recalcitrant carbon collected during the final 850ºC heat treatment (open squares).

bulk untreated soil material is −27.5‰, consistent with a C_3-dominated environment. Organic carbon $\delta^{13}C$ values increase with increasing depth as seen in other studies (Bowen and Beerling, 2004) (Figure 1). At the conclusion of the step-wise dehydration process, a final 850ºC step served to completely dehydrate all remaining gibbsite in the sample (Table 2). The carbon collected during this step may be recalcitrant organic carbon that was not removed during the chemical treatment or the initial oxidation step. The $\delta^{13}C$ value of recalcitrant carbon is used as a proxy for the $\delta^{13}C$ value of the organic material in the soil when using this method to estimate paleo-PCO_2 (Yapp and Poths, 1996). Although the $\delta^{13}C$ values of the 850ºC step are, on average, more depleted than bulk SOM by 3.5‰, with the exception of two samples, the close agreement between the bulk SOM and recalcitrant carbon $\delta^{13}C$ values reinforces the use of this CO_2 as an acceptable estimate for soil organic carbon.

X-ray diffraction analysis further showed that the majority of the <2 μm material in the soil is kaolin and gibbsite with minor amounts of goethite and hydroxy-interlayered vermiculite (HIV) (Figure 2). A mica phase exists in the 0−5 cm and 20−25 cm samples and is indicative of the foliated gneissic parent material. Shallow samples also contained more goethite than the other samples; gibbsite is the dominant oxy-hydroxide phase present, however. The upper 5−10 cm of the soil contained the largest amounts of HIV. The presence of HIV (which can potentially host interlayer organics), along with the greater bulk organic content, accounted for increased yield of CO_2 from the samples taken at shallow depths. CO_2 yields at 0−5 cm varied between 35 and 80 μmoles g^{-1}, whereas at depths >5 cm (when HIV did not dominate the mineral assemblage) yields were <20 μmoles g^{-1} with little variability amongst all deeper samples (Table 3).

To ensure that the CO_2 collected during the dehydration of gibbsite was representative of the trapped CO_2, the ratio of moles of CO_2 to moles of H_2O (F value, nCO_2/nH_2O) was plotted *vs.* the progress of dehydration (Figure 3). As discussed previously, when the CO_2 is released from the mineral structure the F value should remain constant. CO_2 collected from 0−5 cm did not show a constant F value during any part of the dehydration process. Combined with the large and variable CO_2 yield of these samples, the large organic content of the upper 5 cm of the soil, and the presence of HIV, the CO_2 collected is concluded to have originated from multiple sources and the $\delta^{13}C$ values are, therefore, not useful proxies (Figure 3, sample 0005). The rest of the samples did show constant F values and the CO_2 from the plateaus identified were assumed, therefore, to be representative of CO_2 trapped in the gibbsite structure (Figure 3). $\delta^{13}C$ values of the plateaus for the remaining samples showed enrichment from the surface to 40 cm followed by the expected depletion with depth (Figure 1) (Table 2). Similarly, the measured $\delta^{18}O$ values were most enriched at 30 cm and became more depleted with depth. Keeping in mind the caveat that there may be

https://doi.org/10.1346/CCMN.2014.0620402 Published online by Cambridge University Press

Table 1. Percent clay and total carbon and $\delta^{13}C$ values for untreated bulk-soil samples from two cores adjacent to the soil pit and from the soil pit itself.

Sample ID		Depth (cm)	% Clay	% Total C	$\delta^{13}C$ (‰ VPDB)
C11530	Core 1	23	12.2	1.30	−25.78
C14450		47	34.0	0.95	−25.21
C15066		58	41.1	0.43	−24.67
C16682		74	57.0	0.44	−25.25
C18298		90	54.1	0.40	−25.86
C1114130		122	42.3	0.11	−24.35
C1114130		122	24.9	0.12	−23.59
C30005	Core 3	3	6.8	5.71	−27.05
C30515		8		1.53	−26.10
C31524		20	13.4	0.71	−25.43
C32430		27	56.4	0.59	−23.70
C33040		35	62.1	0.43	−22.87
C34047		44	63.1	0.32	−22.61
C35563		59	56.9	0.12	−22.32
C35563		59	40.0	0.12	−22.05
C36370		67	34.9	0.31	−24.02
C37078		74	14.1	0.09	−21.74
C37888		83	20.4	0.13	−21.51
C38895		92	16.9	0.07	−21.55
C395105		100	8.4	0.15	−22.28
C3105115		110	10.2	0.10	−22.28
C3115125		120	15.3	0.09	−21.12
C3125135		130		0.09	−22.10
C3135150		143		0.10	−22.44
FS0005	Soil Pit	3		0.95	−26.07
FS0515		10		0.32	−22.58
FS1020		15		0.25	−20.29
FS2025		23		0.22	−21.55
FS32025		23		0.83	−26.23
FS2535		30		0.17	−17.40
FS3545		40		0.09	−18.03
FS4555		50		0.10	−19.92
FS5575		65		0.10	−20.08
FS5575		65		0.07	−20.07
FS7595		85		0.09	−20.64
FS95105		100		0.09	−20.61

Table 2. Mineral index, plateau $\delta^{13}C$ and $\delta^{18}O$ values of treated samples, and $\delta^{13}C$ values of the 850ºC dehydration step.

Sample ID	Depth (cm)	Mineral index	Plateau $\delta^{13}C$ (‰ VPDB) n	$\delta^{13}C$	s.d.	Plateau $\delta^{18}O$ (‰ VPDB) n	$\delta^{18}O$	s.d.	850ºC $\delta^{13}C$ (‰ VPDB) n	$\delta^{13}C$	s.d.
0005	3	0.13	5	−23.3	2.2	5	−3.3	1.8	4	−24.6	2.2
0515	8	0.24	3	−17.5	2.1	3	−1.8	0.8	2	−26	0.2
1020	15	0.31	3	−15.3	0.3	3	−1.2	1.0	2	−25.1	2.6
2025	23	0.15	3	−21.1	0.4	3	−2.5	0.5	2	−25.2	0.4
2535	30	0.47	3	−16.5	0.6	3	1.3	2.1	3	−19.3	0.7
3545	40	0.44	3	−11.5	0.4	3	0.9	2.9	3	−21.4	0.2
4555	5	0.47	3	−23.1	0.9	3	−3.3	0.4	1	−23.4	
5575	65	0.37	3	−20.4	0.8	3	−2.5	0.8	2	−22.2	0.5
7595	85	0.53	3	−24.2	1.1	3	−5.8	3.9	3	−23.2	1
95105	100	0.44	3	−25.7	0.5	3	−9.2	3.3	3	−23.3	0.7

https://doi.org/10.1346/CCMN.2014.0620402 Published online by Cambridge University Press

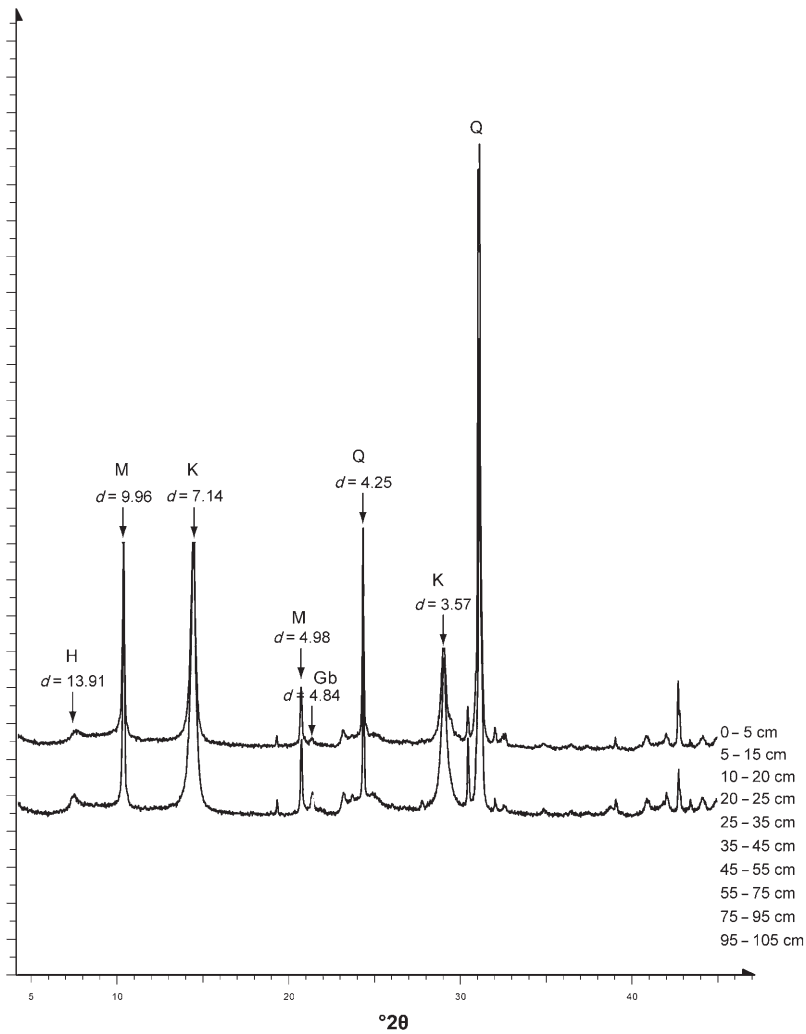

Figure 2. XRD patterns (Co radation) of the <2 μm size fraction of soil material (after chemical treatment). H = hydroxy interlayer vermiculite, M = mica, K = kaolinite, Gb = gibbsite, Q = quartz.

isotope exchange between the CO_2 and H_2O during sample collection, $\delta^{18}O$ values below this depth followed the expected depth profile for diffusion.

Examining the patterns of stable carbon and oxygen isotopic composition trends with depth for the entire soil profile, the one-dimensional (1D) Fickian diffusion-process could not describe the results. Generally, three regions of the soil profile appeared to reflect different carbon occlusion processes. In the upper portion of the soil, above the Bt horizon, the $\delta^{13}C$ values changed from relatively depleted (*i.e.* close to the value of SOM) to a maximum enrichment in the A horizon (15 cm). Values were more depleted near the AB horizon (22 cm). Between the AB and Bt horizons (22−40 cm), there was a large enrichment of ^{13}C with maximum enrichment of both oxygen and carbon isotopes corresponding with the top of the Bt horizon (1.3 and −11.5 VPDB, respectively). At depths > 40 cm, $\delta^{13}C$ values returned to those expected deep in the soil for a 1D Fickian diffusion process.

DISCUSSION

The $\delta^{13}C$ value of CO_2 in the soil pore space is understood to be controlled by the diffusive mixing of CO_2 produced at depth in the soil and CO_2 influx from the atmosphere (Cerling, 1984, 1991; Cerling *et al.*, 1989). CO_2 respired in the soil, by plant roots and microbes, has an initial $\delta^{13}C$ value that corresponds to the photosynthetic pathway used by the plants. The degree of mixing with the atmosphere is determined by the rate of CO_2 flux through the soil. These two factors, therefore, have the greatest degree of influence over final $\delta^{13}C$ value of the pore space CO_2 (Cerling, 1991; Austin, 2011). The soil CO_2 efflux rate is a product of the concentration gradient between the atmosphere and the soil pore space and the tortuosity of the soil pore space.

The $\delta^{18}O$ value of soil CO_2 is also understood to be controlled by the factors discussed above as they affect diffusion in addition to the isotope exchange between

https://doi.org/10.1346/CCMN.2014.0620402 Published online by Cambridge University Press

Table 3. Gibbsite dehydration CO_2 and H_2O yields.

Sample ID	Sample weight (g)	Weight lost (g)	Step	Time (min)	CO_2 yield (μmol)	CO_2 release rate (μmol/min)	H_2O yield (μmol)	F	$\delta^{13}C$	$\delta^{13}C$ s.d.	$\delta^{18}O$	$\delta^{18}O$ s.d.
000501	0.554	0.051	1	45	4.9	0.11	85.8	0.06	−19.4	0.024	−2.3	0.036
			2	45	2.3	0.05	49.1	0.05	−19.9	0.004	−3.3	0.077
			3	45	2.0	0.04	23.6	0.08	−19.4	0.061	−3.6	0.042
			4	60	2.5	0.04	26.9	0.09	−19.6	0.024	−2.7	0.055
			5	120	2.6	0.02	18.6	0.14	−20.9	0.027	−3.8	0.039
			6	59	11.5	0.19	717.1	0.02				
000502	0.731	0.069	1	45	4.8	0.11			−23.1	0.045	−4.6	0.046
			2	45	8.0	0.18	34.6	0.23	−23.0	0.029	−2.3	0.078
			3	45	6.1	0.14	29.2	0.21	−23.8	0.035	−2.1	0.035
			4	60	11.9	0.20	26.8	0.44	−24.7	0.021	−1.8	0.020
			5	120	14.4	0.12	46.3	0.31	−25.0	0.074	−2.1	0.078
			6	30	30.1	1.00	81.0	0.37	−24.7	0.035	−4.6	0.030
000503	0.620	0.058	1	45	6.1	0.14	56.7	0.11	−21.6	0.024	0.1	0.060
			2	45	5.5	0.12	51.5	0.11	−21.1	0.039	−0.1	0.033
			3	45	3.2	0.07			−23.9	0.025	−1.3	0.069
			4	60	6.5	0.11	33.1	0.20	−23.8	0.027	−1.4	0.049
			5	120	8.4	0.07	38.8	0.22	−25.8	0.055	−1.7	0.061
			6	30	31.0	1.03	285.8	0.11	−21.4	0.084	−4.7	0.088
000504	0.508	0.050	1	45	3.0	0.07	24.4	0.12	−24.8	0.048	−6.1	0.058
			2	45	7.5	0.17	39.5	0.19	−24.5	0.019	−5.3	0.023
			3	45	8.0	0.18	36.9	0.22	−24.6	0.016	−5.6	0.033
			4	60	11.4	0.19	35.0	0.33	−24.9	0.029	−7.1	0.044
			5	120	16.0	0.13	44.8	0.36	−25.2	0.015	−7.8	0.028
			6	30	14.0	0.47	51.3	0.27	−26.2	0.022	−9.9	0.028
000505	0.697	0.064	1	45	6.3	0.14	36.5	0.17				
			2	48	8.6	0.18	49.8	0.17	−23.7	0.032	−3.6	0.027
			3	42	5.7	0.14			−24.6	0.028	−3.4	0.055
			4	60	10.9	0.18	43.7	0.25	−25.6	0.044	−4.2	0.045
			5	120	15.4	0.13	44.7	0.34	−25.7	0.055	−3.3	0.031
			6	30	20.7	0.69	62.1	0.33	−26.1	0.024	−5.5	0.049
051501	0.573	0.081	1	45	2.3	0.05	42.5	0.05	−14.3	0.023	−3.4	0.030
			2	45	3.0	0.07	55.3	0.05	−15.3	0.015	−2.6	0.066
			3	45	2.2	0.05	33.1	0.07	−15.0	0.083	−1.8	0.199
			4	60	3.1	0.05			−21.1	0.030	−2.7	0.077
			5	120	6.3	0.05	78.4	0.08	−22.7	0.027	−0.3	0.062
			6	30	6.7	0.22	98.3	0.07	−26.1	0.036	−9.7	0.040
051502	0.541	0.076	1	42	1.8	0.04			−15.6	0.014	−2.6	0.042
			2	48	2.8	0.06	36.3	0.08	−18.0	0.025	−1.0	0.024
			3	45	2.4	0.05	27.1	0.09	−20.2	0.041	−0.2	0.108
			4	60	2.9	0.05	37.8	0.08	−22.7	0.010	−2.7	0.046
			5	120	8.5	0.07						
			6	30								
051503	0.668	0.096	1	45	4.3	0.10	255.9	0.02	−13.9	0.018	−1.1	0.036
			2	45	3.7	0.08	103.9	0.04	−15.1	0.027	−0.7	0.115
			3	45	1.9	0.04	40.6	0.05	−18.3	0.013	−1.0	0.026
			4	60	2.7	0.05	54.0	0.05	−21.6	0.027	−2.6	0.049
			5	120	3.3	0.03	122.6	0.03	−23.8	0.016	−2.5	0.051
			6	30	10.8	0.36	64.7	0.17	−25.8	0.024	−5.2	0.048
102001	0.607		1	45	2.8	0.06			−12.1	0.018	−1.2	0.029
			2	45	3.2	0.07	75.5	0.04	−11.9	0.020	−0.5	0.027
			3	45	1.9	0.04	41.0	0.05	−13.9	0.020	−0.2	0.026
			4	60	2.5	0.04	51.2	0.05	−17.2	0.043	−2.0	0.107
			5	120	2.8	0.02	48.8	0.06				
			6	30	4.4	0.15	48.4	0.09	−23.3	0.014	−7.6	0.025
102002	0.919	0.136	1	45	5.7	0.13	201.1	0.03				
			2	45	6.2	0.14	188.9	0.03	−11.5	0.016	−1.6	0.049
			3	45	2.7	0.06	75.2	0.04	−13.2	0.051	0.3	0.126
			4	60	3.3	0.06	83.9	0.04	−16.7	0.025	−1.4	0.051
			5	120	3.6	0.03	71.5	0.05				
			6	30		0.00	63.2	0.00	−26.9	0.032	−13.7	0.117
102003	0.662	0.098	1	45	2.4	0.05	102.0	0.02	−13.4	0.030	−3.0	0.057
			2	45	4.1	0.09	46.8	0.09	−12.6	0.019	−2.1	0.050
			3	45	3.1	0.07	82.0	0.04	−13.9	0.018	−1.2	0.021
			4	60	2.8	0.05			−17.0	0.033	−2.9	0.032
			5	120	3.3	0.03	75.3	0.04	−18.7	0.033	−1.2	0.094
			6	30								

https://doi.org/10.1346/CCMN.2014.0620402 Published online by Cambridge University Press

Table 3 (*contd*.)

Sample ID	Sample weight (g)	Weight lost (g)	Step	Time (min)	CO_2 yield (μmol)	CO_2 release rate (μmol/min)	H_2O yield (μmol)	F	$\delta^{13}C$	$\delta^{13}C$ s.d.	$\delta^{18}O$	$\delta^{18}O$ s.d.
202501	0.825	0.094	1	45	2.1	0.05	106.1	0.02	−14.9	0.021	−2.0	0.069
			2	45	3.1	0.07	75.1	0.04	−16.4	0.007	−1.7	0.029
			3	45	2.1	0.05	41.0	0.05	−21.2	0.039	−2.8	0.057
			4	60	3.1	0.05			−20.7	0.011	−2.6	0.035
			5	120	3.5	0.03	51.0	0.07	−21.8	0.031	−2.5	0.044
			6	30	7.6	0.25	62.3	0.12	−25.0	0.031	−7.0	0.046
202502	0.578	0.067	1	45	4.5	0.10	229.1	0.02	−14.0	0.045	0.6	0.125
			2	45	2.9	0.06	65.7	0.04	−18.3	0.031	−1.5	0.026
			3	45	1.8	0.04	39.2	0.05				
			4	60	3.6	0.06	56.9	0.06	−20.7	0.018	−2.6	0.035
			5	120	3.5	0.03	42.9	0.08	−20.1	0.017	−3.1	0.022
			6	30	7.5	0.25			−25.5	0.055	−5.8	0.068
202503	0.579	0.067	1	45	1.5	0.03	54.9	0.03	−15.9	0.011	−1.9	0.027
			2	45	2.9	0.06	48.3	0.06	−17.1	0.024	0.8	0.035
			3	45	1.8	0.04	30.3	0.06	−19.1	0.016	−0.1	0.088
			4	60	2.5	0.04	40.8	0.06	−21.5	0.019	−2.5	0.030
			5	120	3.2	0.03	66.2	0.05	−21.5	0.016	−1.4	0.048
			6	30								
253501	0.639	0.149	1	45	2.6	0.06	336.2	0.01	−16.2	0.027	0.5	0.071
			2	45	3.2	0.07	298.6	0.01	−12.0	0.026	1.3	0.039
			3	45	0.7	0.02	27.0	0.03	−14.8	0.018	0.9	0.013
			4	60	1.5	0.03	44.3	0.03	−17.2	0.017	−0.8	0.066
			5	120	2.1	0.02	39.7	0.05				
			6	30	2.8	0.09	35.0	0.08	−19.6	0.014	−4.7	0.068
253502	0.742	0.115	1	45	2.5	0.06	229.0	0.01	−11.0	0.027	4.7	0.043
			2	45	2.3	0.05	98.9	0.02	−11.9	0.036	0.9	0.118
			3	45	1.4	0.03	44.5	0.03	−15.2	0.020	0.9	0.087
			4	60	2.1	0.04			−17.9	0.052	2.0	0.102
			5	120	2.4	0.02			−18.2	0.034	−0.6	0.038
			6	30	6.1	0.20	57.0	0.11	−19.8	0.017	−3.2	0.058
253503	0.909	0.141	1	45	2.2	0.05			−13.1	0.044	2.4	0.094
			2	45	3.5	0.08	72.2	0.05	−14.4	0.043	4.2	0.087
			3	45	2.5	0.06	43.6	0.06	−16.7	0.025	4.8	0.047
			4	60	3.3	0.06	58.0	0.06	−18.5	0.031	2.3	0.042
			5	120	4.0	0.03	57.2	0.07				
			6	30	4.4	0.15	54.2	0.08	−18.5	0.040	−3.0	0.061
354501	0.715	0.115	1	45	2.6	0.06	516.0	0.01	−14.9	0.020	1.9	0.080
			2	45	1.7	0.04	134.2	0.01	−10.9	0.004	1.7	0.018
			3	45	0.6	0.01	38.2	0.02	−17.6	0.016	−1.2	0.030
			4	60	1.0	0.02	63.6	0.02	−13.2	0.030	2.8	0.043
			5	120	1.0	0.01	51.5	0.02	−15.1	0.049	2.4	0.127
			6	30	8.2	0.27	112.1	0.07	−21.5	0.030	−7.4	0.051
354502	0.911	0.326	1	45	3.1	0.07	569.1	0.01	−13.2	0.023	−0.7	0.022
			2	45	1.2	0.03	101.8	0.01	−10.9	0.088	−0.8	0.243
			3	45	0.8	0.02	51.2	0.02	−12.0	0.026	0.7	0.042
			4	60	1.1	0.02	82.0	0.01	−13.5	0.033	−3.1	0.048
			5	120								
			6	30	25.1	0.84			−21.5	0.023	−7.5	0.065
455501	0.833		1	45	2.0	0.04	49.5	0.04	−18.2	0.005	−2.0	0.049
			2	45	1.6	0.04	53.0	0.03	−20.8	0.009	−3.1	0.023
			3	45	1.0	0.02	29.1	0.03	−22.5	0.015	−1.6	0.029
			4	60	1.8	0.03	40.1	0.04	−24.5	0.024	−4.0	0.071
			5	120	1.9	0.02	32.9	0.06	−23.8	0.010	−2.3	0.022
			6	30								
455502	0.983	0.148	1	45	1.0	0.02	60.8	0.02				
			2	45	2.1	0.05	44.0	0.05	−22.0	0.027	−3.1	0.016
			3	45	1.2	0.03	31.9	0.04	−24.9	0.033	−3.5	0.076
			4	60	2.3	0.04	41.1	0.06	−25.5	0.006	−4.4	0.053
			5	120	2.4	0.02	39.6	0.06	−23.7	0.011	−4.4	0.017
			6	30	14.5	0.48	24.5	0.59				
455503	1.038	0.160	1	45	1.6	0.04	52.0	0.03	−19.3	0.021	−2.7	0.011
			2	45	2.1	0.05	42.6	0.05	−21.6	0.022	−3.5	0.013
			3	45	1.4	0.03	36.5	0.04	−22.7	0.021	−3.4	0.032
			4	60	2.4	0.04	45.2	0.05	−23.6	0.024	−4.0	0.062
			5	120	2.4	0.02	42.3	0.06	−22.4	0.027	−3.2	0.045
			6	30	7.7	0.26	38.0	0.20	−23.4	0.057	−8.3	0.062

https://doi.org/10.1346/CCMN.2014.0620402 Published online by Cambridge University Press

Table 3 (*contd*.)

Sample ID	Sample weight (g)	Weight lost (g)	Step	Time (min)	CO_2 yield (μmol)	CO_2 release rate (μmol/min)	H_2O yield (μmol)	F	$\delta^{13}C$	$\delta^{13}C$ s.d.	$\delta^{18}O$	$\delta^{18}O$ s.d.
557501	0.935	0.128	1	35	0.7	0.02	39.5	0.02	−19.0	0.011	−2.9	0.024
			2	45	0.8	0.02	25.4	0.03	−20.9	0.037	−2.5	0.015
			3	45	0.8	0.02	34.3	0.02	−21.6	0.022	−1.4	0.019
			4	60								
			5	120	1.3	0.01	28.7	0.05	−21.2	0.040	−2.4	0.126
			6	30	2.0	0.07	19.7	0.10	−22.5	0.013	−9.0	0.025
557502	1.033	0.147	1	45	0.8	0.02	45.9	0.02	−18.1	0.029	−2.6	0.091
			2	45	1.2	0.03	39.7	0.03	−19.1	0.040	−2.6	0.059
			3	45	0.9	0.02	32.7	0.03	−19.8	0.021	−1.6	0.066
			4	60	1.1	0.02	37.8	0.03	−21.1	0.025	−3.2	0.132
			5	120	1.3	0.01	34.6	0.04	−20.4	0.002	−2.4	0.031
			6	30	1.6	0.05	24.5	0.07	−21.9	0.036	−7.5	0.108
557503	0.940	0.120	1	45								
			2	45	0.3	0.01			−19.7	0.009	−3.4	0.029
			3	45	0.4	0.01			−20.0	0.050	6.5	0.129
			4	60	0.2	0.00			−22.6	0.023	−4.3	0.014
			5	120	0.2	0.00			−21.5	0.038	−3.0	0.083
			6	30	0.2	0.01						
759501	1.005	0.111	1	45	2.4	0.05			−19.7	0.016	−2.1	0.037
			2	45	2.8	0.06			−21.3	0.017	−1.9	0.061
			3	45	0.4	0.01			−24.1	0.067	−2.9	0.170
			4	60	2.2	0.04			−24.5	0.022	−4.0	0.040
			5	120	3.6	0.03			−21.8	0.059	−3.8	0.195
			6	30	6.4	0.21			−22.4	0.043	−6.5	0.026
759502	0.916	0.145	1	45	3.8	0.08			−21.5	0.012	−4.1	0.026
			2	45	1.5	0.03			−25.5	0.023	−8.6	0.023
			3	45	0.4	0.01			−25.5	0.045	−10.3	0.046
			4	60	1.1	0.02			−24.5	0.036	−13.1	0.122
			5	120	1.2	0.01			−23.3	0.037	−13.6	0.060
			6	30	28.0	0.93						
759503	0.976	0.156	1	45	3.7	0.08			−21.9	0.011	−1.4	0.027
			2	45	1.9	0.04			−30.3	0.055	−9.4	0.139
			3	45	1.4	0.03			−23.8	0.006	−3.5	0.028
			4	60	0.6	0.01			−22.3	0.032	−5.1	0.086
			5	120	9.2	0.08			−19.1	0.043	−0.1	0.069
			6	30	28.0	0.93			−22.9	0.029	−11.0	0.051
9510501	0.977	0.142	1	45	2.8	0.06			−19.7	0.017	−4.8	0.041
			2	45	1.1	0.02			−26.1	0.021	−7.1	0.045
			3	45	0.9	0.02			−26.2	0.046	−4.8	0.089
			4	60	1.2	0.02			−26.1	0.008	−5.5	0.040
			5	120	1.3	0.01			−23.4	0.013	−6.2	0.034
			6	30	28.0	0.93			−24.0	0.060	−10.1	0.080
9510502	0.999	0.145	1	45	2.9	0.06			−19.6	0.012	−7.1	0.037
			2	45	1.0	0.02			−26.4	0.167	−13.0	0.250
			3	45								
			4	60	0.9	0.02			−23.9	0.038	−12.4	0.100
			5	120	0.9	0.01			−21.8	0.024	−11.1	0.042
			6	30					−23.4	0.022	−10.2	0.035
9510503			1	45	2.9	0.06			−19.5	0.019	−6.9	0.030
			2	45	0.9	0.02						
			3	45	0.8	0.02			−26.0	0.031	−9.5	0.022
			4	60	0.9	0.02			−25.6	0.050	−11.3	0.141
			5	120	1.0	0.01			−23.8	0.013	−12.4	0.100
			6	30								

https://doi.org/10.1346/CCMN.2014.0620402 Published online by Cambridge University Press

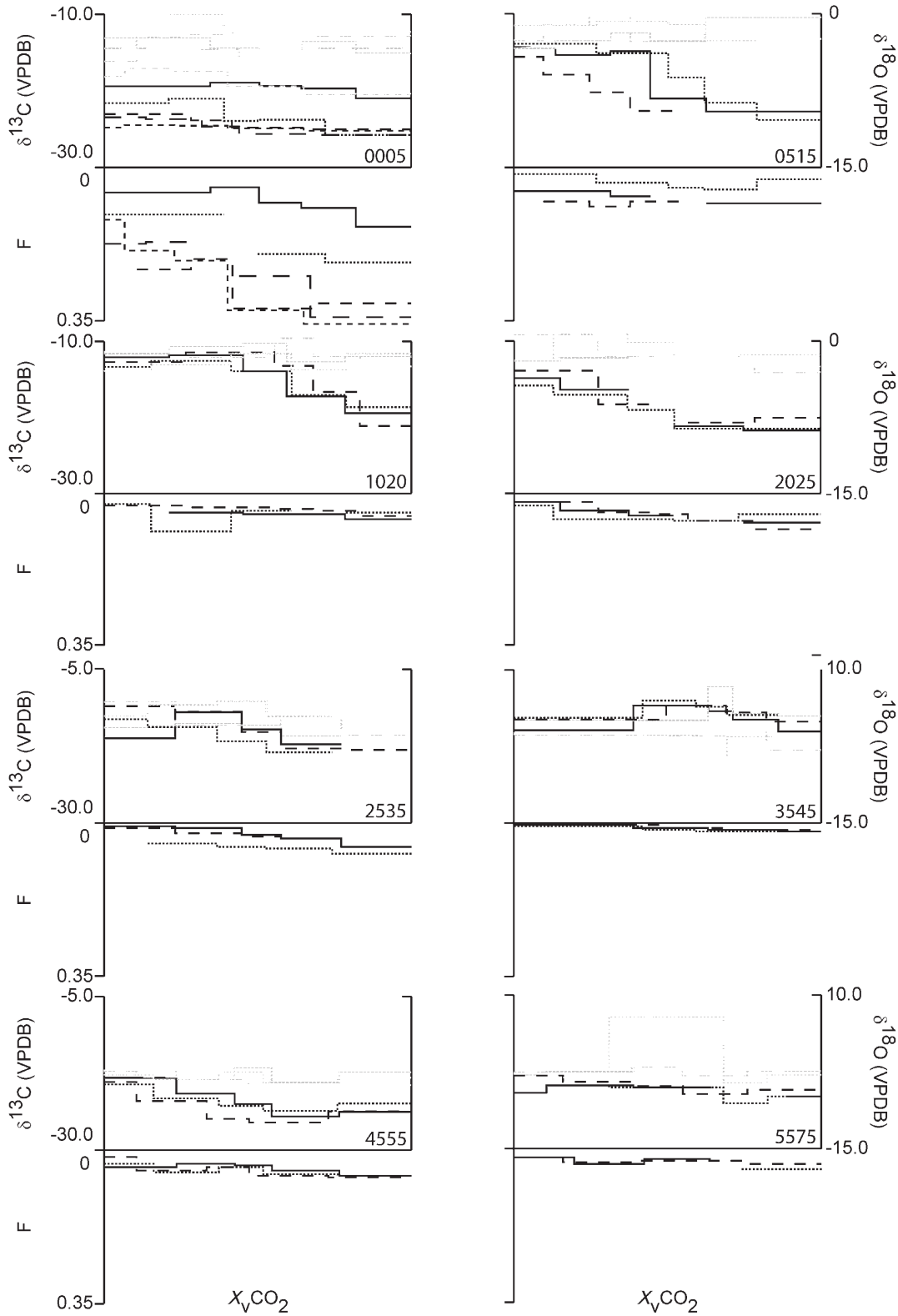

Figure 3. Dehydration and decarbonation steps for sample replicates. Solid, dashed, and dotted lines represent xxxx01, xxxx02, and xxxx03, respectively, where xxxx is the sample ID as labeled on each horizontal axis (see also Table 3). X_vCO_2 is the fraction of the total CO_2 yield at each step. $\delta^{13}C$ is plotted in black and $\delta^{18}O$ is plotted in gray.

https://doi.org/10.1346/CCMN.2014.0620402 Published online by Cambridge University Press

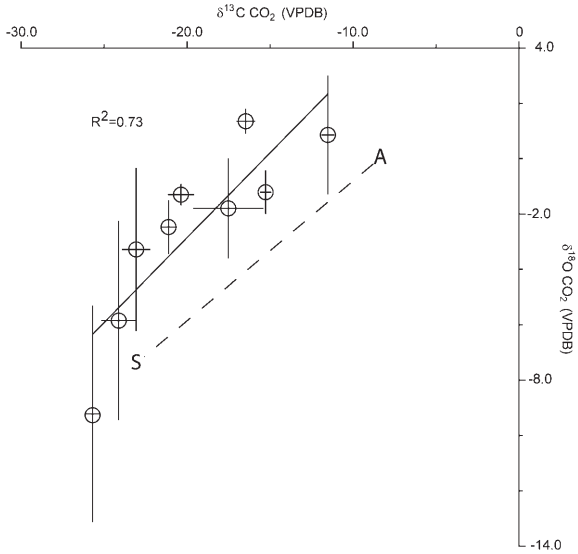

Figure 4. $\delta^{13}C$ *vs.* $\delta^{18}O$ of the plateau samples for each depth. Error bars represent one standard deviation of all plateau samples at each depth (Figure 3), $R^2 = 0.73$ ($p < 0.01$). S represents the average SOM value as determined by all samples collected during the 850ºC heat treatment in the dehydration procedure. A represents an average value for atmospheric CO_2 (Chen *et al.*, 2013). The line between atmosphere and SOM is arbitrary and represents linear mixing between the two reservoirs.

soil CO_2 and H_2O (Stern *et al.*, 1999). Because the factors affecting these two isotopes are similar, correlation between the $\delta^{13}C$ and $\delta^{18}O$ values of CO_2 occluded in the gibbsite structure with a possible shift in the $\delta^{18}O$ value due to isotope exchange seems likely. A linear relationship existed between the $\delta^{13}C$ and $\delta^{18}O$ values of CO_2 measured in this study ($R^2 = 0.73$) (Figure 4) and was offset roughly parallel to a hypothetical mixing line between the atmosphere (Chen *et al.*, 2013) and the SOM, indicating that the process was controlled by diffusion. A process other than diffusion must be responsible for the offset, however.

Fractionation resulting from oxygen exchange between the CO_2 and transition states as the CO_2 moves through the mineral structure during dehydration must be considered. Fractionation of oxygen isotopes of CO_2 occluded in goethite has been modeled as a function of the reaction rate, where the greatest extent of fractionation occurs in association with slow reaction rate (Yapp, 2003). Gibbsite dehydration was assumed to proceed *via* a similar process, by the reaction

$$2Al(OH)_3 \rightarrow 2AlO(OH)^* + 2H_2O \rightarrow 2AlO(OH)^* \rightarrow Al_2O_3 + H_2O \quad (5)$$

where AlO(OH)* represents a transition state. A reasonable inference is that a similar reaction rate-controlled fractionation might occur. Using the method described by Yapp (2003), $\ln Xs(H_2)$ was plotted *vs*. the cumulative reaction time to determine the reaction rate (Figure 5). $X_s(H_2)$ was used to determine the progress of the reaction and is defined as the fraction of the total H_2 remaining in the sample. All samples in this study showed very similar reaction rates. If it was further assumed that the magnitude of fractionation for gibbsite was similar to goethite for a given difference in reaction rate, the measured $\delta^{18}O$ values relative to each other were expected to be within 1‰ of the relative values of the original unfractionated CO_2 $\delta^{18}O$ values. Therefore,

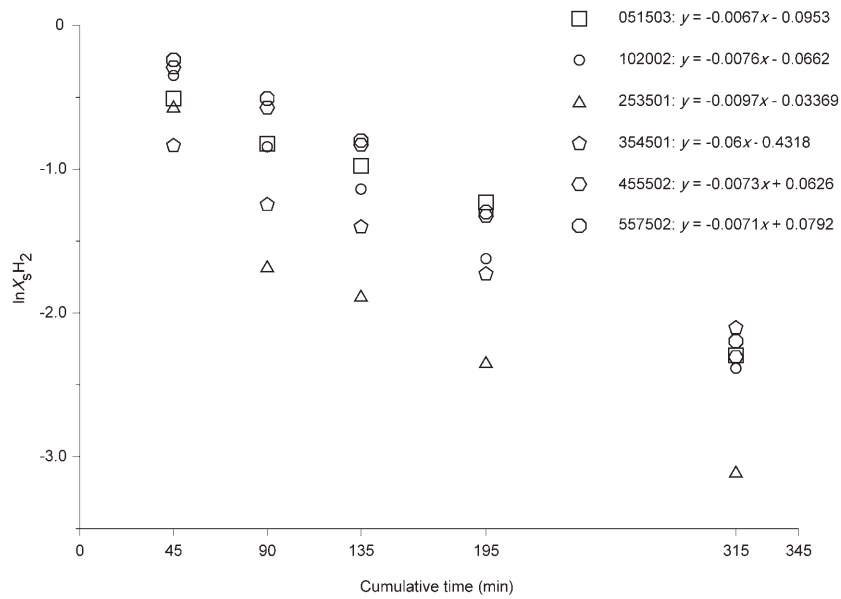

Figure 5. $\text{Ln}X_s(H_2)$ *vs*. cumulative dehydration time for gibbsite samples 051503, 102002, 253501, 35450, 455502, and 557502. R^2 for all samples >0.97 except 253501 ($R^2 = 0.92$) and 354501 ($R^2 = 0.86$). See Yapp (2003) and the text.

https://doi.org/10.1346/CCMN.2014.0620402 Published online by Cambridge University Press

while the absolute values measured were not useful, the relative values were, and were used to establish the relationship between $\delta^{13}C$ and $\delta^{18}O$. Until the structural $\delta^{18}O$ value of gibbsite is measured, this discussion will continue using these assumptions.

In addition to fractionation during dehydration, the difference between the measured mixing line and the theoretical mixing line could represent isotope exchange between CO_2 and H_2O in the soil pore space prior to inclusion in the mineral structure. As shown by Stern (1999), the amount of exchange is dependent on the residence time of the CO_2 in the soil pore space. Therefore, the degree of change from the assumed pore space CO_2 $\delta^{18}O$ value may have implications for inferring the soil diffusion conditions during mineral formation. For example, a relatively small difference between the mixing line for atmosphere and SOM may represent high soil respiration rates, precluding isotope exchange. Conversely, a large shift implies a slow respiration rate, allowing for more isotope exchange. Until the reality of fractionation during sample collection is resolved, exchange and diffusion fractionation effects cannot be quantified.

Finally, the $\delta^{18}O$ value of SOM or the atmosphere or both may change over time. Determining the magnitude of change was complicated by the uncertainty of the sequence of formation and transport of gibbsite in the soil compared to the age of the active soil-forming processes. Cosmogenic ^{10}Be estimates of the soil residence time of the Southern Piedmont ranged between 1.3 and 3.1 million years (Bacon *et al*., 2012). Radiogenic carbon dates of pedogenic gibbsite measured at Panola Mountain, Georgia showed at least two distinct populations deep in the soil on a millennial time scale (Schroeder *et al*., 2001). Differences between mineral 'ages' and soil residence time suggested that mineral populations are reforming continuously in the soil. Therefore, CO_2 occluded in gibbsite near the surface should be representative of the relatively recent past environment (*i.e.* <10,000 y). Atmospheric CO_2 $\delta^{13}C$ has been depleted by ~1.2‰ over the past 250 y (post-industrial revolution) by the release of depleted organic carbon into the atmosphere by the burning of fossil fuels (Francey *et al*., 1999). $\delta^{18}O$ of atmospheric CO_2 for time scales of soil formation is influenced by climate, as it relates to changes in precipitation, and the carbon cycle, as it relates to changes in plant type and respiration (Welp *et al*., 2011).

While the correlation between $\delta^{13}C$ and $\delta^{18}O$ values indicated that diffusion was controlling the isotopic compositions of soil CO_2, the depth profile of $\delta^{13}C$ values did not match the progressive decrease with depth expected in a diffusion-controlled profile. The depth profile of $\delta^{13}C$ values in the upper 40 cm showed an erratic increase from the surface to the top of the Bt horizon. At depths >40 cm, the profile appears to follow the expected diffusion-controlled profile. This implies that there is some process other than diffusion controlling the profile shape above the Bt horizon. Because the correlation of $\delta^{13}C$ and $\delta^{18}O$ implied that diffusion was the controlling process and the $\delta^{13}C$ values of the gibbsite-occluded CO_2 at 40 cm are most similar to the atmosphere, the implication is that transport and mixing of gibbsite above the Bt horizon is responsible for the unexpected depth profile. Mixing in the upper portion made utilization of the pedogenic gibbsite proxy more difficult but may provide insight into the processes and timing of events in soils regarding dissolution, formation, and transport, particularly in deep intensely weathered soils. Measuring the radiocarbon content of occluded gibbsite CO_2 and its distribution down profile will provide insight into the extent of mixing recorded by the gibbsite at different depths in the soil.

Regarding the preservation of a weathering profile in the rock record (*i.e.* a paleosol), carbon-rich, poorly consolidated O, A, and upper AB horizons are likely to have low preservation potential. Thus, paleosols preserved in the rock record were probably decapitated during the erosional and subsequent depositional events that deposited unconformable sequences above. The more clay-rich lower AB and Bt horizons are more likely to be preserved. If these horizons are studied for their gibbsite CO_2 $\delta^{13}C$ values, the mixing curve (*i.e.* asymptotic values are approached with depth) still potentially harbors information about the original SOM pool and the atmosphere with which it mixed. The key to using gibbsite preserved in ancient soil is observing the soil textural properties to be sure about the horizons being sampled. The USDA-ARS study site used here is unique in that the only mixing of the soil has been bioturbation and tree-throw (no tilling). Also minimized at this site was the introduction of an enriched C_4 carbon pool. The present authors suggest that the signal recorded and preserved here reflects a more pre-human like condition, where rapid erosion or changes in carbon input have probably not taken place. In contrast, most landscapes in the southeastern United States have experienced intense cultivation, which affects mixing and can lead to erosion of the A horizon and its gibbsite-hosted carbon signal (*i.e.* accelerated erosion). Human-induced factors have not been considered in previous occluded gibbsite carbon studies, which were sampled at a site that probably did undergo significant erosion and agricultural tilling (Schroeder and Melear, 1999). For this reason, managed, tilled, and eroded landscapes, with a concentration of enriched carbon isotopes at the top of the preserved Bt horizon, may serendipitously appear more like a paleosol than an undisturbed soil.

CONCLUSIONS

Co-variation of the stable carbon and oxygen isotopic composition of carbonate occluded in the pedogenic gibbsite structure parallel to a mixing line between the

https://doi.org/10.1346/CCMN.2014.0620402 Published online by Cambridge University Press

atmosphere and SOM indicates that the process which controls these compositions is probably diffusive mixing. The difference in the depth profile of measured $\delta^{13}C$ values and the expected diffusion-controlled profile suggests that other transport processes have occurred after mineral formation. In the shallow soil active mixing by physical or biological processes makes interpretation of the depth profile of stable carbon isotope composition difficult. As a result, care should be taken when using paleosol proxies to identify the soil type and horizons, especially in soils with Bt horizons which indicate a concentration of alluvial clay, or with A, E, or B horizons which may be mixed due to bioturbation. Restricting samples to the region below the Bt horizon removes the upper portion of the profile, which allows for more precise PCO_2 estimates, but until the systematics of mixing can be determined and modeled reliably, estimates using deep soil only will have errors comparable to current paleosol methods.

ACKNOWLEDGMENTS

The authors thank Julie Cox for her help with the redesign of the isotope extraction line, which was essential to the success of this project. The manuscript was improved significantly by the thoughtful comments of two anonymous reviewers. Support was provided by The Clay Minerals Society, NSF-EAR-0501690, EAR-IF-0929912, and EAR-1331846.

REFERENCES

Austin, J.C. (2011) Soil CO_2 efflux simulations using Monte Carlo method and implications for recording paleo-atmospheric PCO_2 in pedogenic gibbsite. *Palaeogeography Palaeoclimatology Palaeoecology*, **305**, 280–285.

Bacon, A.R., Richter, D.D., Bierman, P., and Rood, D.H. (2012) Coupling meteoric ^{10}Be with pedogenic losses of ^{9}Be to improve soil residence time estimates on an ancient North American interfluve. *Geology*, **40**, 847–850.

Berner, R.A. and Kothavala, Z. (2001) GEOCARB III: A revised model of atmospheric CO_2 over Phanerozoic time. *American Journal of Science*, **301**, 182–204.

Bowen, G.J. and Beerling, D.J. (2004) An integrated model for soil organic carbon and CO_2: Implications for paleosol carbonate pCO_2 paleobarometry. *Global Biogeochemical Cycles*, **18**, GB1026 1021–1012.

Breecker, D.O., Sharp, Z.D., and McFadden, L.D. (2009) Seasonal bias in the formation and stable isotopic compostition of pedogenic carbonate in modern soils from central New Mexico, USA. *Geological Society of America Bulletin*, **121**, 630–640.

Cerling, T.E. (1984) The stable isotopic composition of modern soil carbonate and its relationship to climate. *Earth and Planetary Science Letters*, **71**, 229–240.

Cerling, T.E. (1991) Carbon dioxide in the atmosphere: evidence from Cenozoic and Mesozoic Paleosols. *American Journal of Science*, **291**, 377–400.

Cerling, T.E., Quade, J., and Bowman, J.R. (1989) Carbon isotopes in soils and palaeosols as ecology and palaeoecology indicators. *Nature*, **341**, 138–139.

Chen, Q., Zhu, R., and Xu, H. (2013) Stable isotopes of carbon dioxide in the marine atmosphere along a hemispheric course from China to Antartica. *Atmospheric Environment*, **80**, 342–346.

Cuntz, M., Ciais, P., Hoffmann, G., and Knorr, W. (2003) A comprehensive global three-dimensional model of $\delta^{18}O$ in atmospheric CO_2: 1. Validation of surface processes. *Journal of Geophysical Research*, **108**, 4528, doi: 10.1029/2002JD003153.

Farrimond, P., Eglinton, G., and Brassell, S.C. (1986) Alkenones in Cretaceous black shales, Blake-Bahama Basin, western North Atlantic. *Organic Geochemistry*, **10**, 897–903.

Francey, R.J., Allison, C.E., Etheridge, D.M., Trudinger, C.M., Enting, I.G., Leuenberger, M., Langerfelds, R.L., Michel, E., and Steele, L.P. (1999) A 1000-year high precision record of $\delta^{13}C$ in atmospheric CO_2. *Tellus*, **51B**, 170–193.

Freeman, K.H. and Hayes, J.M. (1992) Fractionation of carbon isotopes by phytoplankton and estimates of ancient CO_2 levels. *Global Biogeochemical Cycles*, **6**, 185–198.

Hesterberg, R. and Siegenthaler, U. (1991) Production and stable isotopic composition of CO_2 in a soil near Bern, Switzerland. *Tellus*, **43B**, 197–205.

Hsieh, J.C.C., Savin, S.M., Kelly, E.F., and Chadwick, O.A. (1998) Measurement of soil-water $\delta^{18}O$ values by direct equilibration with CO_2. *Geoderma*, **82**, 255–268.

Kump, L.R. and Arthur, M.A. (1999) Interpreting carbon-isotope excursions: carbonates and organic matter. *Chemical Geology*, **161**, 181–198.

Kurschner, W.M., Van Der Burgh, J., Visscher, H., and Dilcher, D.L. (1996) Oak leaves as biosensors of late Neogene and early Pleistocene paleoatmospheric CO_2 concentrations. *Marine Micropaleontology*, **27**, 299–312.

Marlowe, I.T., Brassell, S.C., Eglinton, G., and Green, J.C. (1990) Long-chain alkenones and alkyl alkenoates and the fossil coccolith record of marine sediments. *Chemical Geology*, **88**, 349–375.

Miller, J.B., Yakir, D., White, J.W.C., and Tans, P.P. (1999) Measurement of $^{18}O/^{16}O$ in the soil-atmosphere CO_2 flux. *Global Biogeochemical Cycles*, **13**, 761–774.

Pagani, M., Freeman, K.H., and Arthur, M.A. (1999) Late Miocene atmospheric CO_2 concentrations and the expansion of C_4 grasses. *Science*, **285**, 876–879.

Robertson, S.M. (1968) Soil Survey of Clarke and Oconee Counties, Georgia. Department of Agriculture, U.S.A.

Royer, D.L., Berner, R.A., and Beerling, D.J. (2001) Phanerozoic atmospheric CO_2 change: evaluating geochemical and paleobiological approaches. *Earth Science Reviews*, **54**, 349–392.

Schroeder, P.A. and Melear, N.D. (1999) Stable carbon isotope signatures preserved in authigenic gibbsite from a forested granitic-regolith: Panola Mountain, Georgia, USA. *Geoderma*, **91**, 261–279.

Schroeder, P.A., Melear, N.D., Bierman, P., Kashgarian, M., and Caffee, M.W. (2001) Apparent gibbsite growth ages for regolith in the Georgia Piedmont. *Geochimica et Cosmochimica Acta*, **65**, 381–386.

Schroeder, P.A., Austin, J.C., and Dowd, J.F. (2006) Estimating long-term soil respiration rates from carbon isotopes occluded in gibbsite. *Geochimica et Cosmochimica Acta*, **70**, 5692–5697.

Stern, L., Baisden, W.T., and Amundson, R. (1999) Processes controlling the oxygen isotope ratio of soil CO_2: Analytic and numerical modeling. *Geochimica et Cosmochimica Acta*, **63**, 799–814.

Su, C.M. and Suarez, D.L. (1997) In situ infrared speciation of absorbed carbonate on aluminum and iron oxide. *Clays and Clay Minerals*, **45**, 814–825.

Tabor, N.J. and Yapp, C.J. (2005) Incremental vacuum dehydration-decarbonation experiments on a natural gibbsite (α-$Al(OH)_3$): CO_2 abundance and $\delta^{13}C$ values. *Geochimica et Cosmochimica Acta*, **69**, 519–527.

Van Der Burgh, J., Visscher, H., Dilcher, D.L., and Kurschner,

W.M. (1993) Paleoatmospheric signatures in Neogene fossil leaves. *Science*, **260**, 1788–1790.

Welp, L.R., Keeling, R.F., Meijer, H.A.J., Bollenbacher, A.F., Piper, S.C., Yoshimura, K., Francey, R.J., Allison, C.E., and Wahlen, M. (2011) Interannual variability in the oxygen isotopes of atmospheric CO_2 driven by El Nino. *Nature*, **477**, 579–582.

Woodward, F.I. and Bazzaz, F.A. (1988) The responses of stomatal density to CO_2 partial pressure. *Journal of Experimental Botany*, **39**, 1771–1781.

Yapp, C.J. (1997) An assessment of isotopic equilibrium in goethites from a bog iron deposit in a lateritic regolith. *Chemical Geology*, **135**, 159–171.

Yapp, C.J. (2003) A model for $^{18}O/^{16}O$ variations in CO evolved from goethite during the solid-state α-FeOOH to α-Fe_2O_3 phase transition. *Geochimica et Cosmochimica Acta*, **67**, 1991–2004.

Yapp, C.J. and Poths, H. (1986) Carbon in natural goethites. *Geochimica et Cosmochimica Acta*, **50**, 1213–1220.

Yapp, C.J. and Poths, H. (1990) Infrared spectral evidence for a minor Fe(III) carbonate bearing component in natural goethite. *Clays and Clay Minerals*, **38**, 442–444.

Yapp, C.J. and Poths, H. (1992) Ancient atmospheric CO_2 pressures inferred from natural goethites. *Nature*, **355**, 342–344.

Yapp, C.J. and Poths, H. (1996) Carbon isotopes in continental weathering environments and variations in ancient atmospheric CO_2 pressure. *Earth and Planetary Science Letters*, **137**, 71–82.

(*Received 1 April 2014; revised 2 September 2014; Ms. 755; AE: H. Dong*)